J Appl Electrochem (2014) 44:53–60
DOI 10.1007/s10800-013-0599-1

RESEARCH ARTICLE

Nanorod-like Fe_2O_3/graphene composite as a high-performance anode material for lithium ion batteries

Bing Zhao · Ruizhe Liu · Xinhui Cai · Zheng Jiao · Minghong Wu · Xuetao Ling · Bo Lu · Yong Jiang

Received: 27 May 2013 / Accepted: 3 August 2013 / Published online: 14 August 2013

Abstract In this study, a nanorod-like Fe_2O_3/graphene nanocomposite is synthesized by a facile template-free hydrothermal method and a following calcination in air at 300 °C for 2 h. The Fe_2O_3 nanorods with diameter of 15–30 nm and length of 120–300 nm are homogenous distributed on both sides of graphene. The morphologies of intermediates at different hydrothermal reaction times are investigated by transmission electron microscopy (TEM) characterization, and a possible growth mechanism of this one-dimensional structure is proposed. It is shown that the α-FeOOH rodlike precursors are formed through a rolling-broken-growth (RBG) model, then the α-FeOOH is transformed into α-Fe_2O_3 nanorods during calcinations, preserving the same rodlike morphology. Electrochemical characterizations demonstrate that the Fe_2O_3 nanorod/graphene composites exhibit a very large reversible capacity of 1063.2 mAh/g at the charge/discharge rate of 0.1 C.

Keywords Iron oxide · Graphene · Anode material · Lithium ion battery

1 Introduction

Recently, the increasing demands on portable, high-performance energy storage devices have stimulated intense research interests in energy areas, such as lithium ion batteries (LIBs) and electrochemical capacitors [1–3].

Nanomaterials of metal oxides, such as SnO_2 [4], Mn_3O_4 [5], NiO [6] and Fe_2O_3 [7, 8], have been intensively exploited as anode materials for lithium ion batteries because of their high theoretical specific capacities. Compared to other transition metals and metal oxides, hematite α-Fe_2O_3 has been suggested as a promising anode candidate for rechargeable lithium ion batteries basically owing to its much higher theoretical specific capacity (ca. 1007 mAh/g) than commercial graphite (372 mAh/g), high abundance, low cost, non-toxicity and environmental benignity [9, 10]. However, its Li-ion storage properties, especially high rate performance, are still limited because of its poor electrical conductivity and the large volume expansion/shrinkage which can cause structure collapse during the Li-ion reactions with α-Fe_2O_3 [11–13].

To solve this problem, graphene (GNS) based on transition metal oxides [14–16] have drawn a great deal of researches and are expected to show improved cycling performance and high rate capability owing to their enhanced electrical conductivity, due to graphene materials possess excellent electrical conductivity, mechanical stability and large surface areas [17, 18]. Integrating graphene into functional architectures and composites currently has been an active research field. Up to now, a number of researches have been reported recently for graphene-based Fe_2O_3 composites, such as nanoparticles, nanorice, nanotubes and nanorods [15, 19–21]. The specific capacity and cycling performances of these nanocomposites were substantially increased compared with bare iron oxides anodes. Meanwhile, extensive research efforts have demonstrated that intriguing properties and applications may be generated by tailoring the shape and size of functional Fe_2O_3 nanomaterials. However, to the best of our knowledge,

B. Zhao · R. Liu · X. Cai · Z. Jiao · M. Wu · X. Ling · Y. Jiang (✉)
School of Environmental and Chemical Engineering, Shanghai University, Shanghai 200444, People's Republic of China
e-mail: jiangyong@shu.edu.cn

B. Lu
Instrumental Analysis and Research Center, Shanghai University, Shanghai 200444, People's Republic of China

there are few researches studying on growth mechanism of iron oxide on graphene surface.

This paper proposes an environmentally friendly and quick strategy for the synthesis of α-FeOOH nanorods/graphene composite via a low-temperature hydrothermal technique. Through heating the as-obtained α-FeOOH nanorods/graphene precursor at 300 °C for 2 h, α-Fe_2O_3 nanorods/graphene could be obtained, preserving the same rodlike morphology. The growth mechanism of the nanocomposites was investigated by intercepting the intermediates at different hydrothermal reaction times. It is shown that the one-dimensional nanostructure was formed via a RBG process [22, 23]. The electrochemical experiments showed that the as-obtained Fe_2O_3 nanorods/graphene exhibited a large reversible capacity of 1063.2 mAh/g at 0.1 C rate (based on the total mass of the hybrid material) as well as good rate capability, which were significantly enhanced compared with that of bare Fe_2O_3.

2 Experimental

2.1 Synthesis of graphene

Graphene oxide (GO) sheets were prepared from natural graphite powder via a modified Hummers method as described in our previous work [14]. Typically, graphite powder (3 g) was put into an 80 °C solution of concentrated H_2SO_4 (12 mL), $K_2S_2O_8$ (2.5 g) and P_2O_5 (2.5 g). The mixture was kept at 80 °C for 4 h and then cooled to room temperature, diluted with deionized water (DI, 0.5 L) and left overnight. The mixture was centrifuged, washed with DI water and dried. The preoxidized graphite was further oxidized in concentrated H_2SO_4 (120 mL) and $KMnO_4$ (15 g) for 2 h under stirring and cooling conditions. Then, the mixture was diluted with DI water (250 mL) in an ice bath to keep the temperature below 50 °C for 2 h and further diluted with DI water (700 mL); 30 % H_2O_2 (20 mL) was then added to the mixture, and a brilliant yellow product was formed. The product was centrifuged and washed with 1:10 HCl (1 L) aqueous solution and DI water (1 L) to remove the metal ions and acid. The resulting GO sheets were dried at 80 °C in a vacuum.

GO sheets (0.2 g) were thermally reduced in a simple horizontal tube furnace in a nitrogen atmosphere with heating rate of 5 °C/min at 500 °C for 2 h. After pyrolytic reduction, the final black powders were GNS.

2.2 Synthesis of Fe_2O_3/graphene

In a typical synthesis process, 0.05 g as-synthesized graphene was dissolved in 30 mL of DI water by ultrasonication to form a suspension. This suspension was mixed with 40 mL of 0.278 g $Fe_2SO_4{\cdot}7H_2O$ and 0.328 g CH_3COONa aqueous solution under constant stirring. After stirring vigorously in air for 20 min, the mixture suspension was then transferred into 100 mL Teflons and heated at 100 °C for 8 h. The autoclave was then cooled to room temperature naturally. The final black solid products were centrifuged and washed with DI water and absolute ethanol several times and then dried at 60 °C under vacuum for 12 h. The Fe_2O_3 nanorods/graphene were obtained by heating the as-obtained α-FeOOH nanorods/graphene in air at 300 °C for 2 h. In a control experiment, we synthesized free Fe_2O_3 nanorods by the same method without any graphene added.

2.3 Materials characterizations

The obtained products were characterized by X-ray diffraction (XRD, Rigaku D/max-2550 V, Cu Kα radiation), field-emission scanning electron microscopy (FE-SEM, JSM-6700F) with an energy dispersive X-ray spectrometer (EDS) and transmission electron microscopy/selected area electron diffraction (TEM/SAED, JEOL JEM-200CX and JEM-2010F) in the Instrumental Analysis and Research Center, Shanghai University. The carbon contents in the final anode materials were determined by Carbon & Sulfur Determinator (CS444LSc).

2.4 Electrode fabrication and electrochemical measurements

The working electrodes were prepared by mixing 80 wt % active materials, 10wt % acetylene black and 10wt % polytetrafluoroethylene (PTFE). The lithium metal foil was used as the anode, while the electrolyte was a solution of 1 M $LiPF_6$ in dimethyl carbonate (DMC) and ethylene carbonate (EC) (1:1 by weight). The Swagelok-type cell was assembled in an argon-filled glove box and tested on a LAND CT2001A cell test system with galvanostatic charge and discharge in the voltage range of 5 mV–3.0 V (*vs.* Li/Li^+) at different current densities (0.1 C-1 C rate, 1 C = 1000 mA/g) at room temperature.

3 Results and discussion

Figure 1a is the XRD pattern of the as-prepared FeOOH/graphene precursor, where all the diffraction peaks could be indexed as pure orthorhombic α-FeOOH (JCPDS 29-0713, lattice constant $a = 4.610$ Å, $b = 9.556$ Å and $c = 3.024$ Å). The wide peak at 24.9° can be indexed to (002) plane of hexagonal graphite structure, which suggests that graphene was successfully introduced into the composite. After heating the as-obtained α-FeOOH nanorods/graphene at 300 °C

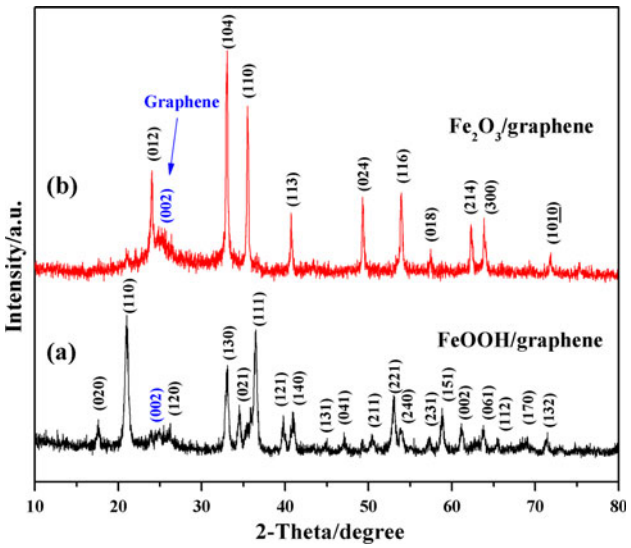

Fig. 1 X-ray diffraction patterns of *a* α-FeOOH nanorods/graphene and *b* Fe_2O_3 nanorods/graphene composites

for 2 h, a few characteristic peaks such as (012), (104), (110) and (116) planes could be readily indexed to the standard hematite α-Fe_2O_3 (JCPDS 33-0664. $a = 5.035$ Å, $b = 5.035$ Å and $c = 13.749$ Å) (Fig. 1b), and no obvious diffraction peaks of α-FeOOH appear, indicating that the product is completely transformed to α-Fe_2O_3 after calcination.

Figure 2 shows the Raman spectra of graphene and Fe_2O_3 nanorods/graphene composite. There are two characteristic peaks at 1340 and 1592 cm^{-1} for Fe_2O_3/graphene composite, which correspond to the D band (κ-point phonons of A_{1g} symmetry) and G band (E_{2g} phonon of C sp^2 atoms) of graphene. Besides the two peaks, the Raman band at 225 cm^{-1} is assigned to A_{1g} mode and the bands at

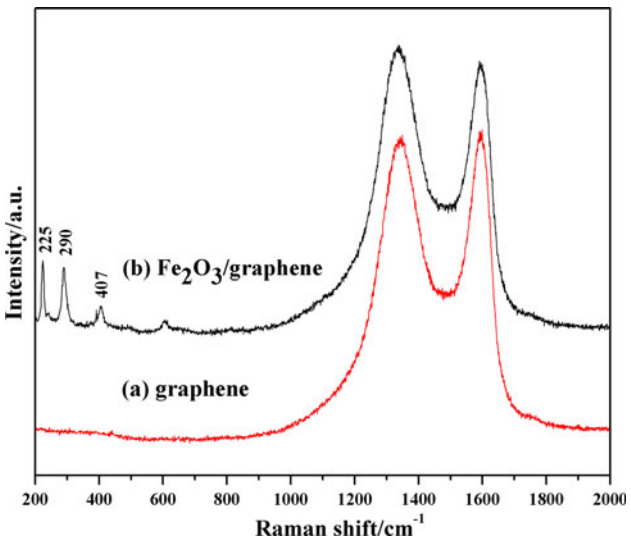

Fig. 2 Raman spectra of *a* graphene and *b* Fe_2O_3 nanorods/graphene composites

290 and 407 cm^{-1} are assigned to E_g vibration modes of hematite. Such a result confirms that Fe_2O_3/graphene nanocomposite has been obtained. The intensity ratio of D and G bands (I_D/I_G) was calculated to be 1.06 for Fe_2O_3 nanorods/graphene, higher than that of graphene (0.99). This more disordered carbon structure in the Fe_2O_3/graphene composites compared with bare GNS may be due to the possible insertion of Fe_2O_3 nanorods into GNS layers [24]. This agrees well with the previous observation on NiO/graphene composite [21]. A large number of defects or cavities may be generated on the surface of GNS, which could be applied to store an extra number of lithium ions.

The morphologies of as-prepared Fe_2O_3 and Fe_2O_3/graphene are examined by SEM and TEM characterizations. Fig. 3a and 3b is the low- and high-magnification TEM images of the as-obtained pure Fe_2O_3 nanorods, and it can be seen clearly that the as-obtained pure Fe_2O_3 nanorods have diameters of 15–30 nm and lengths of 120–300 nm. Fig. 3c and 3d shows the SEM and TEM images of Fe_2O_3 nanorods/graphene composite prepared in the presence of graphene by a similar procedure. Due to the corrugated nature of the disordered graphene nanosheet, the Fe_2O_3 nanorods are homogeneously distributed on the curly surface of the graphene nanosheet. The SEM image of Fe_2O_3/graphene shows that the typical diameter and length of Fe_2O_3 nanorods on graphene are roughly the same as that of pure Fe_2O_3 nanorods, which can be further confirmed by the TEM image in Fig. 3d. The graphene is of inherent wrinkled or crumpled thin voilelike structures with folds, which are mainly due to removal of O-containing groups during the pyrolysis process through the release of CO and CO_2 gases. From the TEM image of nanocomposite, it can be also seen that some Fe_2O_3 nanorods are brighter than others, which seem to be covered by a voilelike GNS. It can be proposed that the Fe_2O_3 nanorods appear on both sides of the support: Some locate above the graphene nanosheet, while others lie on the back of the sheet. It is worthwhile to note that the interaction between nanorods and GNS is quite strong. The intimate contact between the Fe_2O_3 nanorods and graphene sheets enables fast electronic and ionic transport through the active materials to charge collector and thus improves the electrochemical performance. Moreover, Fe_2O_3 nanorods on the surface of GNS can act as spacers to efficiently prevent the aggregation of the nanorods as well as the restacking of graphene sheets, avoiding/weakening the loss of their high active surface area.

The α-FeOOH nanorods/graphene precursor synthesized via a solution chemical route can be illustrated by two processes. (i) Room-temperature reaction. It is well known that GNS offers considerable functional groups such as carboxyl (–COOH) and hydroxyl (–OH) groups on the surface, which makes GNS negatively charged. Fe^{2+} ions are selectively

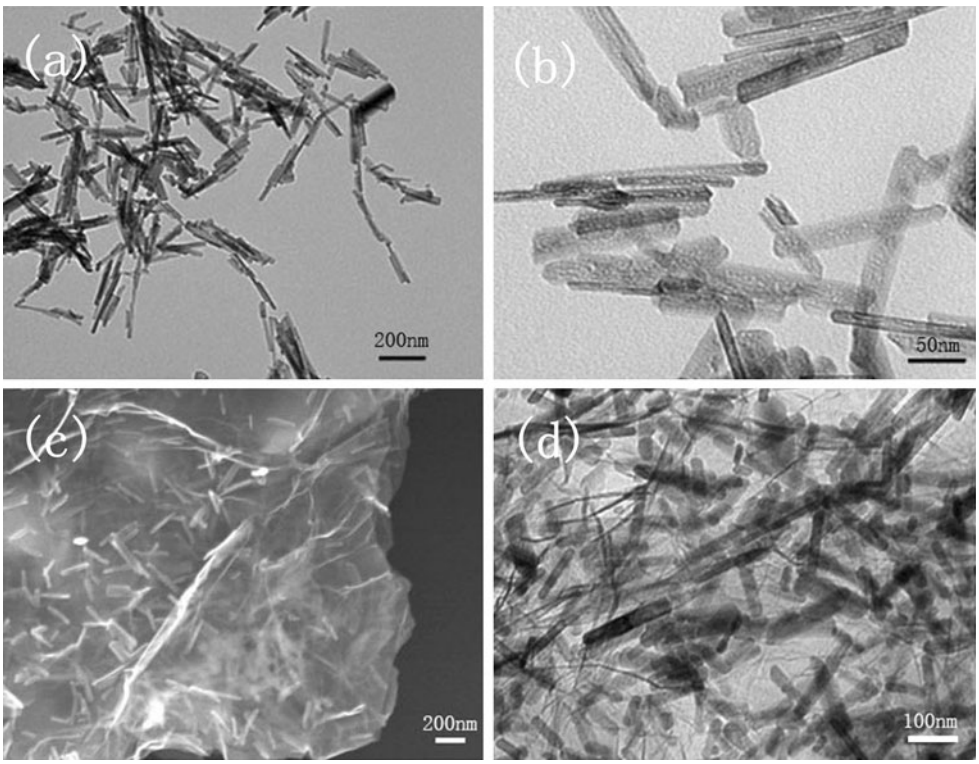

Fig. 3 **a**, **b** TEM images of pure Fe_2O_3 nanorods. **c** SEM and **d** TEM image of Fe_2O_3 nanorods/graphene

bonded with carboxyl through mutual electrostatic attraction. Then, the adsorbed ferrous ions react with OH^- (produced by the hydrolysis of CH_3COO^-) and O_2 at room temperature through the following equation.

$$CH_3COO^- + H_2O \rightarrow CH_3COOH + OH^- \quad (1)$$

$$4Fe^{2+} + 8OH^- + O^2 \rightarrow 4FeOOH + 2H_2O \quad (2)$$

As the reaction proceeded, a black suspension of amorphous FeOOH depositing on both sides of the graphene sheets was obtained. (ii) Hydrothermal reaction. Formation mechanism of the α-FeOOH nanorods/graphene has been investigated via TEM examinations of the intermediates at different hydrothermal reaction times for 0 min, 15 min, 30 min and 1 h, respectively. As shown in the Fig. 4a, a large amount of amorphous flake structures attached on graphene surfaces were obtained before hydrothermal reaction. After heating for 15 min, the thin flakes gradually curled lengthwise into tube shape under the elevated temperature and pressure, as shown in Fig. 4b. As the reaction went on, the long tube broke into short nanotube and further curled driven from the minimization of surface energy, leading to a decrease in average diameters for the nanotubes (Fig. 4c, after heating for 30 min). And finally, small nanotubes would grow into nanorods after heating for 1 h (Fig. 4d). According to the results of these experiments, we believe that the α-FeOOH nanorods/graphene are formed via a RBG model, which is consistent with the previous reported MnO_2 3D nanostructures and CdSe nanorods [22, 23].

In order to study the influence of the CH_3COONa relative content on the morphology and microstructure of the final products in our synthetic system, a series of experiments involved different molar ratios of CH_3COONa to $FeSO_4$ varied from 4 to 1 were performed, keeping the amounts of $FeSO_4$ and GNS constant. When the $CH_3COONa/FeSO_4$ ratio was 4, Fe_2O_3 nanorods with length/diameter aspect ratio larger than 8 were obtained, as shown in Fig. 3c. With CH_3COONa content decreasing (i.e., $CH_3COONa/FeSO_4 = 2$), the Fe_2O_3 nanorods on graphene became short with diameter about 30 nm and length of 100–150 nm and were partial fragmented (Fig. 5a). When CH_3COONa–$FeSO_4$ ratio was further decreased to 1:1, under which condition nanoparticles were obtained (Fig. 5b). So, we conclude that the molar ratio of CH_3COONa to $FeSO_4$ was directly responsible for the morphology of final product, and CH_3COONa can be considered as director agent which has a pronounced influence on the uniformity of as-grown one-dimensional nanorods.

The decoration of α-Fe_2O_3 nanorods on GNS was visibly influenced by the initial weight ratio of $FeSO_4 \cdot 7H_2O$/GNS. When the ratio was increased to 11.1:1 (denoted as Fe_2O_3/GNS_{II}, as seen in Fig. 6), in comparison with the weight ratio of 5.6:1 (Fe_2O_3/GNS_I, Fig. 3c), the quantity of Fe_2O_3 nanorods deposited on graphene increased obviously and the shape became less regular. A few nanorods were stacked together and not contacted with graphene while some nanorods shattering outside of graphene, which may cause the decline of electrochemical properties. The compositions

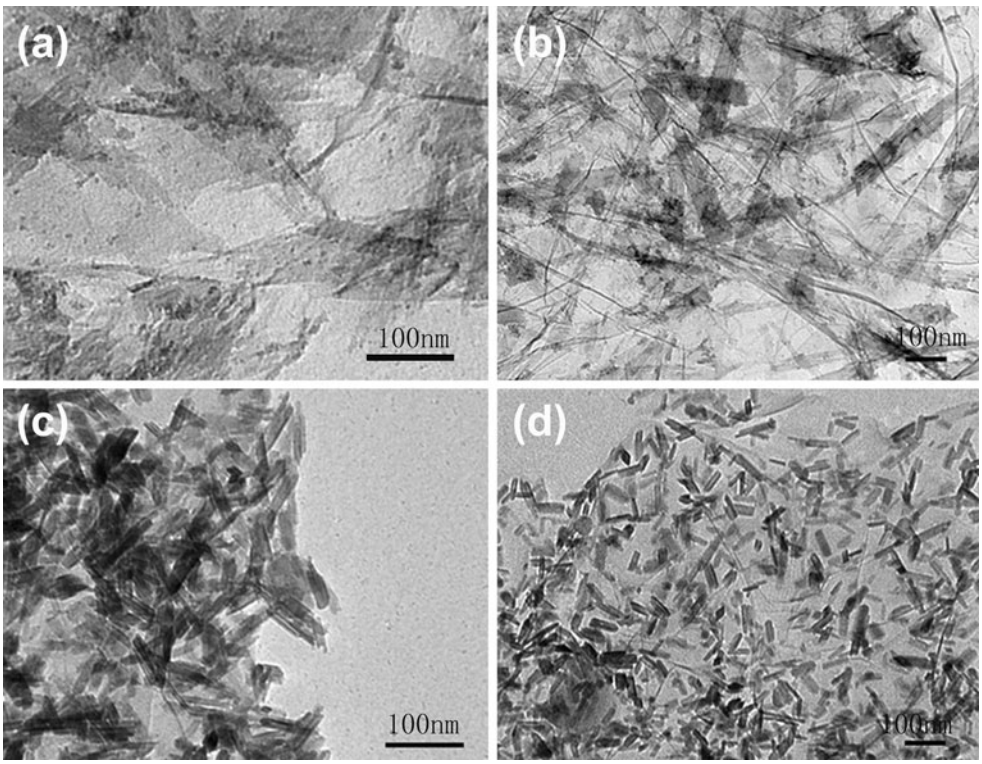

Fig. 4 TEM images of α-FeOOH/graphene at different hydrothermal reaction time intervals: **a** 0 min, **b** 15 min, **c** 30 min and **d** 1 h

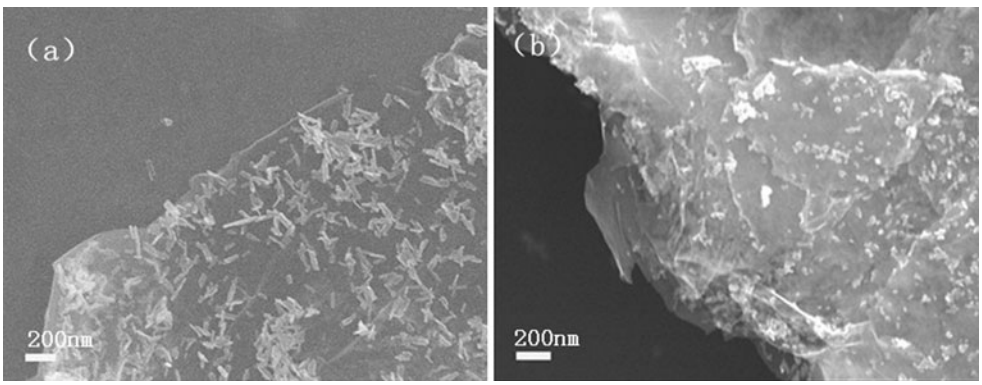

Fig. 5 SEM images of final products at different molar ratio of CH_3COONa to $FeSO_4$: **a** $CH_3COONa:FeSO_4 = 2$ and **b** $CH_3COONa:FeSO_4 = 1$

of two Fe_2O_3/graphene nanocomposites were measured by a high-frequency infrared Carbon & Sulfur Determinator. The carbon contents were determined to be 41.7 and 30.4 % for Fe_2O_3/GNS_I and Fe_2O_3/GNS_{II}, respectively. These values were slightly different with the theoretical value in two Fe_2O_3/GNS composites.

Figures 7a, b shows the first, second and fifth charge–discharge curves of the Fe_2O_3/GNS_I composite and pure Fe_2O_3 nanorods samples at a constant current (0.1 C = 100 mA/g) in the voltage range of 5 mV to 3 V. It was found that the shape of the two curves is very similar, implying that the graphene does not change the lithium storage nature of Fe_2O_3. It is obvious that there are two voltage plateaus at around 1.61 V and 0.78 V in the first discharge curves. As reported in the literature, the voltage plateau at around 1.61 V can be described as a small amount of lithium insertion into the crystal structure of Fe_2O_3 before the structural transformation of the close-packed anionic array from hexagonal to cubic stacking occurs. And the long plateau at approximately 0.78 V reflects the reversible reaction between cubic $Li_2Fe_2O_3$ and Fe [25, 26]. The initial discharge specific capacities of the Fe_2O_3/GNS_I composite (based on the total mass of the hybrid material) and pure Fe_2O_3 nanorods at 0.1 C rate are

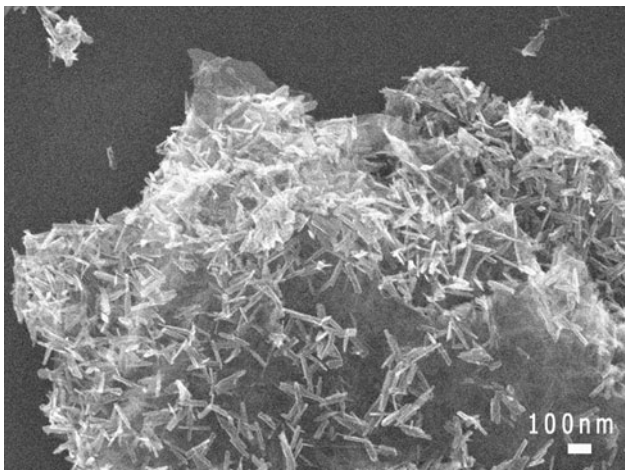

Fig. 6 SEM image of Fe_2O_3/GNS_{II} nanocomposite

1734.6 and 1741.9 mAh/g, respectively, both of which are far exceed to the theoretical capacity (1007 mAh/g) of Fe_2O_3 in this voltage range. The phenomenon that the first discharge capacity considerably exceeds the theoretical capacity has been widely reported for graphene-based transition metal oxides. Usually, the exceeded capacity is ascribed to the electrolyte being reduced at low voltage (generally below 0.8 V *vs.* Li/Li^+) to form a solid electrolyte interphase (SEI) layer and possibly interfacial lithium storage [27–29]. The corresponding reversible charge capacities for these two samples are 1063.2 and 938.9 mAh/g, respectively. After four discharge and charge cycles, the discharge capacity of Fe_2O_3/GNS_I composite is 1042.0 mAh/g, while that of the pure Fe_2O_3 nanorods has decreased to 665.8 mAh/g. The confinement effect and excellent electrical conductivity of GNS obviously play an important role [15, 30].

The rate capabilities and high rate cycling performances of Fe_2O_3/graphene composite and pure Fe_2O_3 nanorods are also investigated and shown in Fig. 7c. Fe_2O_3/GNS_I composite shows rather good rate capability with an average charge capacity of 963.5 mAh/g at a rate of 0.1 C, 651.6 mAh/g at 0.2 C, 353.5 mAh/g at 0.5 C, 210.7 mAh/g at 1 C and finally resumes 616.5 mAh/g when the rate is reduced back to 0.1 C, while pure Fe_2O_3 nanorods exhibit limited

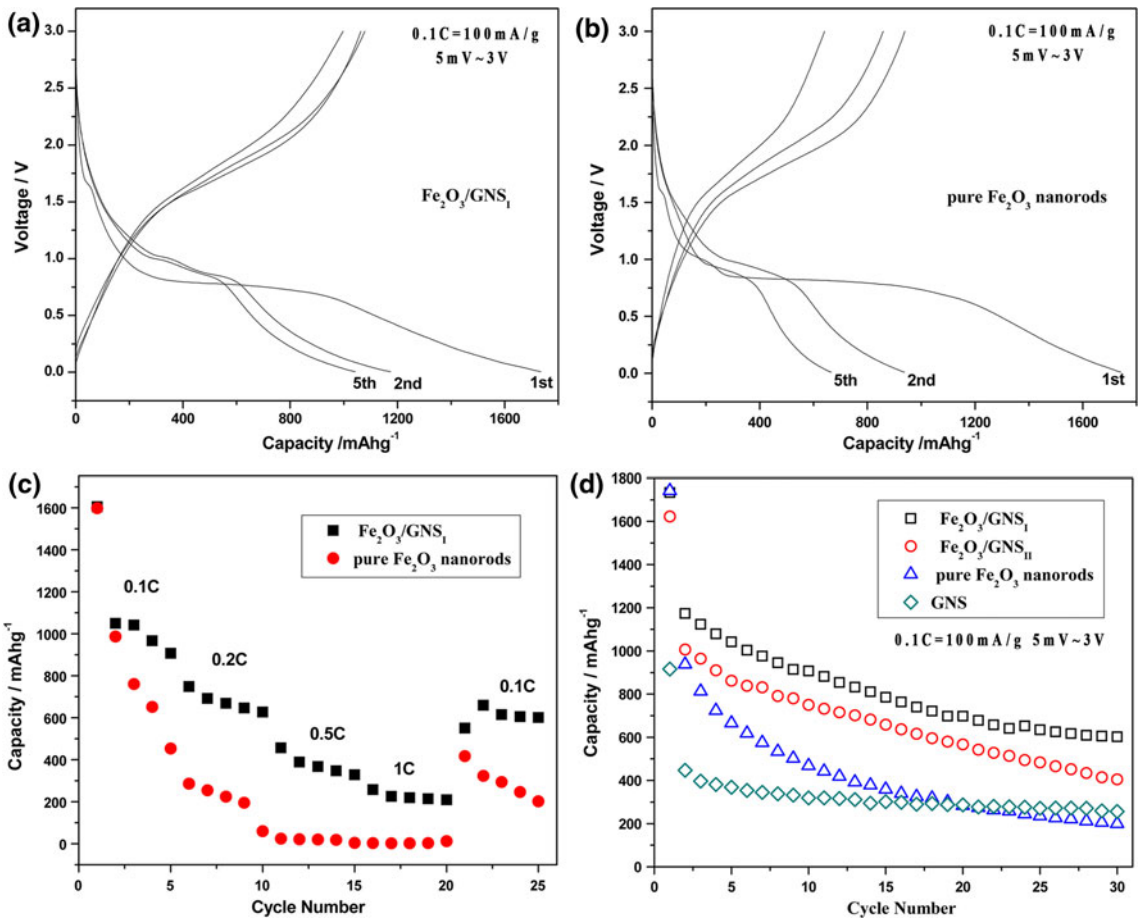

Fig. 7 The first, second and fifth charge–discharge curves of **a** Fe_2O_3 nanorods/graphene composites and **b** pure Fe_2O_3 nanorods. **c** Comparison of rate capability of the Fe_2O_3/GNS_I and pure Fe_2O_3 nanorods. **d** The cycling performances Fe_2O_3/GNS_I, Fe_2O_3/GNS_{II}, pure Fe_2O_3 nanorods and GNS at 0.1 C rate in the voltage range of 5 mV–3.0 V

charge capacities of 890, 147.9, 18.56 and 8.9 mAh/g at the corresponding rates, respectively. The above results demonstrated that the incorporation of GNS had improved the electrochemical properties of Fe_2O_3 as anodes because GNS had built up the interleaved electron transfer highways and excellent Li^+ transport.

Figure 7d shows the cycling performances of the four materials in the voltage range of 5 mV–3.0 V at 0.1 C rate. For pure Fe_2O_3 nanorods and GNS, the discharge specific capacities fade down to 199.1 and 256.5 mAh/g after 30 cycles, respectively. Compared with the above two samples, Fe_2O_3/GNS_I and Fe_2O_3/GNS_{II} could still retain a specific capacity of 602.2 and 404.6 mAh/g after 30 cycles. The enhancement of capacity should be readily attributed to the flexibility of graphene beneficial to structural stability for the electrode during cycle performances. It should also be noted that Fe_2O_3/GNS_I exhibits higher specific capacity and better cycling performance than Fe_2O_3/GNS_{II}, which is in good agreement with our conjecture that stack of nanorods and non-contact with graphene will cause the capacity fade. This side fact indicates that the confinement effect and excellent electrical conductivity of GNS obviously play an important role during the process of discharge and charge.

4 Conclusions

In summary, we have developed a facile and template-free route for the synthesis of nanorod-like Fe_2O_3/graphene composites under hydrothermal conditions. In addition, the growth mechanism of composites was discussed by intercepting the intermediates at different hydrothermal reaction times. The Fe_2O_3 nanorods/graphene composite was found to be more suitable for reversible lithium ion storage compared with pure Fe_2O_3 nanorods. It showed a high reversible capacity of 1063.2 mAh/g and enhanced rate capability. We ascribed the enhancement to the presence of GNS and their high electrical conductivity and mechanical stability. Our simple synthesis method can be readily adapted to prepare other transition metal oxides/graphene composites and be applied in LIBs.

Acknowledgments This work is supported by the Natural Science Foundation of China (11275121, 21241002), Science and Technology Committee of Shanghai (11DZ110020, 13DZ1200502 and 13XD14 24600) and Shanghai Leading Academic Disciplines Project (S30109).

References

1. Yang Y, McDowell MT, Jackson A, Cha JJ, Hong SS, Cui Y (2010) New nanostructured Li_2S/Silicon rechargeable battery with high specific energy. Nano Lett 10:1486–1491
2. Ji XL, Lee KT, Nazar LF (2009) A highly ordered nanostructured carbon–sulphur cathode for lithium–sulphur batteries. Nat Mater 8:500–506
3. Tian L, Zhuang Q, Li J, Wu C, Shi Y, Sun S (2012) The production of self-assembled Fe_2O_3–graphene hybrid materials by a hydrothermal process for improved Li-cycling. Electrochim Acta 65:153–158
4. Meduri P, Pendyala C, Kumar V, Sumanasekera GU, Sunkara MK (2009) Hybrid tin oxide nanowires as stable and high capacity anodes for Li-ion batteries. Nano Lett 9:612–616
5. Wang HL, Cui LF, Yang Y, Casalongue HS, Robinson JT, Liang YY, Cui Y, Dai HJ (2010) Mn_3O_4–graphene hybrid as a high-capacity anode material for lithium ion batteries. J Am Chem Soc 132:13978–13980
6. Varghese B, Reddy MV, Yanwu Z, Lit CS, Hoong TC, Rao GVS, Chowdari BVR, Wee ATS, Lim CT, Sow CH (2008) Fabrication of NiO nanowall electrodes for high performance lithium ion battery. Chem Mater 20:3360–3367
7. Wu CZ, Yin P, Zhu X, OuYang CZ, Xie Y (2006) Synthesis of hematite (α-Fe_2O_3) nanorods: Diameter-size and shape effects on their applications in magnetism, lithium ion battery, and gas sensors. J Phys Chem B 110:17806–17812
8. Larcher D, Bonnin D, Cortes R, Rivals I, Personnaz L, Tarascon JM (2003) Combined XRD, EXAFS, and Mossbauer studies of the reduction by lithium of α-Fe_2O_3 with various particle sizes. J Electrochem Soc 150:A1643–A1650
9. Amatucci GG, Pereira N (2007) Fluoride based electrode materials for advanced energy storage devices. J Fluorine Chem 128:243–262
10. Wang SQ, Zhang JY, Chen CH (2010) Fe_3O_4 submicron spheroids as anode materials for lithium-ion batteries with stable and high electrochemical performance. J Power Sources 195:5379–5381
11. Chen J, Xu LN, Li WY (2005) α-Fe_2O_3 nanotubes in gas sensor and lithium-ion battery applications. Adv Mater 17:582–586
12. Wu XL, Guo YG, Wan LJ, Hu CW (2008) α-Fe_2O_3 nanostructures: Inorganic salt-controlled synthesis and their electrochemical performance toward lithium storage. J Phys Chem C 112:16824–16829
13. Liu H, Wang G, Park J, Wang J, Liu H (2009) Electrochemical performance of α-Fe_2O_3 nanorods as anode material for lithium-ion cells. Electrochim Acta 54:1733–1736
14. Zhao B, Song JS, Liu P, Xu WW, Fang T, Jiao Z, Zhang HJ, Jiang Y (2011) Monolayer graphene/NiO nanosheets with two-dimension structure for supercapacitors. J Mater Chem 21:18792–18798
15. Lee K, Deng S, Fan H, Mhaisalkar S, Tan H, Tok E, Loh K, Chin W, Sow C (2012) α-Fe_2O_3 nanotubes-reduced graphene oxide composites as synergistic electrochemical capacitor materials. Nanoscale 4:2958–2961
16. Chen D, Tang LH, Li JH (2010) Graphene-based materials in electrochemistry. Chem Soc Rev 39:3157–3180
17. Wang GX, Wang B, Wang XL, Park J, Dou SX, Ahn H, Kim K (2009) Sn/graphene nanocomposite with 3D architecture for enhanced reversible lithium storage in lithium ion batteries. J Mater Chem 19:8378–8384
18. Wang GX, Shen XP, Yao J (2009) Graphene nanosheets for enhanced lithium storage in lithium ion batteries. Carbon 47:2049–2053
19. Zhu J, Zhu T, Zhou XZ, Zhang YY, Lou XW, Chen XD, Zhang H, Hng HH, Yan QY (2011) Facile synthesis of metal oxide/reduced graphene oxide hybrids with high lithium storage capacity and stable cyclability. Nanoscale 3:1084–1089
20. Zhu X, Zhu Y, Murali S, Stoller MD, Ruoff RS (2011) Nanostructured reduced graphene oxide/Fe_2O_3 composite as a high-performance anode material for lithium ion batteries. ACS Nano 5:3333–3338
21. Zou YQ, Kan J, Wang Y (2011) Fe_2O_3-graphene rice-on-sheet nanocomposite for high and fast lithium ion storage. J Phys Chem C 115:20747–20753
22. Wu CZ, Xie Y, Wang D, Yang J, Li TW (2003) Selected-control hydrothermal synthesis of γ-MnO_2 3D nanostructures. J Phys Chem B 107:13583–13587

23. Yang J, Zeng JH, Yu SH, Yang L, Zhou G, Qian YT (2000) Formation process of CdS nanorods via solvothermal route. Chem Mater 12:3259–3263
24. Zhang M, Lei D, Chen YJ, Yu XZ, Wang YG (2012) A green and fast strategy for the scalable synthesis of Fe_2O_3/graphene with significantly enhanced Li-ion storage properties. J Mater Chem 22:3868–3874
25. Larcher D, Masquelier C, Bonnin D, Chabre Y, Masson V, Leriche JB, Tarascon JM (2003) Effect of particle size on lithium intercalation into α-Fe_2O_3. J Electrochem Soc 150:A133–A139
26. Wu XL, Guo YG, Wan LJ, Hu CW (2008) α-Fe_2O_3 nanostructures: Inorganic salt-controlled synthesis and their electrochemical performance toward lithium storage. J Phys Chem C 112: 16824–16829
27. Balaya P, Li H, Kienle L, Maier J (2003) Fully reversible homogeneous and heterogeneous Li storage in RuO_2 with high capacity. Adv Funct Mater 13:621–625
28. Morimoto H, Tobishima SI, Iizuka Y (2005) Lithium intercalation into α-Fe_2O_3 obtained by mechanical milling of α-FeOOH. J Power Sources 146:315–318
29. Hang BT, Doi T, Okada S, Yamaki J (2007) Effect of carbonaceous materials on electrochemical properties of nano-sized Fe_2O_3-loaded carbon as a lithium battery negative electrode. J Power Sources 174:493–500
30. Wang DH, Choi DW, Li J, Yang ZG, Nie ZM, Kou R, Hu DH, Wang CM, Saraf LV, Zhang JG, Aksay IA, Liu J (2009) Self-assembled TiO_2–graphene hybrid nanostructures for enhanced Li-ion insertion. ACS Nano 3:907–914